iScience

CellPress
OPEN ACCESS

Article

Live-cell imaging-based dynamic vascular formation assay for antivascular drug evaluation and screening

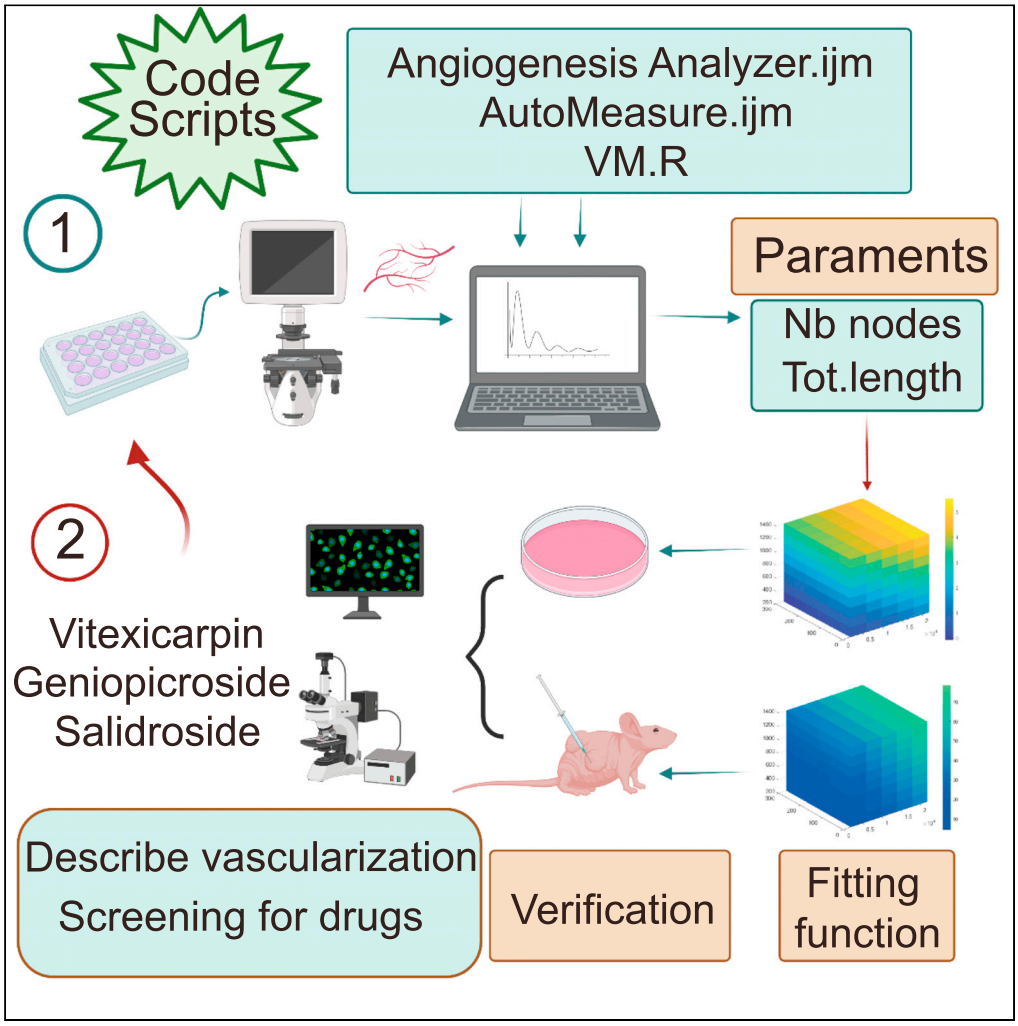

Zhiyang Li, Heng Zhang, Yujie Sun, ..., Yinan Li, Huijuan Liu, Tao Sun

liuhuijuanxyz@163.com (H.L.)
sunrockmia@hotmail.com (T.S.)

Highlights

Automatic analysis of dynamic vascular formation process

Scientific screening of key measurement parameters

The fitting function predicts the vascular formation ability and helps drug screening

Li et al., iScience 26, 106721
May 19, 2023
https://doi.org/10.1016/j.isci.2023.106721

iScience

CellPress
OPEN ACCESS

Article

Live-cell imaging-based dynamic vascular formation assay for antivascular drug evaluation and screening

Zhiyang Li,[1] Heng Zhang,[1] Yujie Sun,[1] Zhuangzhuang Feng,[1] Bijia Cui,[1] Jingxia Han,[1] Yinan Li,[1] Huijuan Liu,[1,*] and Tao Sun[1,2,*]

SUMMARY

New vessel formation (angiogenesis) is an essential physiological process for embryologic development, normal growth, and tissue repair. Angiogenesis is tightly regulated at the molecular level. Dysregulation of angiogenesis occurs in various pathologies and is one of the hallmarks of cancer. However, most existing methods for evaluating cell vascular formation are limited to static analysis and prone to bias due to time, field of vision, and parameter selection. Code scripts, such as AngiogenesisAnalyzer.ijm, AutomaticMeasure.ijm, and VM.R., were developed to study the dynamic angiogenesis process. This method was used to screen drugs that could affect the time, maximum value, tilt, and decline rate of cell vascular formation and angiogenesis. Animal experiments have confirmed that these drugs could inhibit the formation of blood vessels. This work provides a new perspective for the research of angiogenesis process and is helpful to the development of drugs related to angiogenesis.

INTRODUCTION

Dysregulation of angiogenesis is a key feature of many pathological processes, especially processes in tumor tissues.[1–3] The angiogenesis of tumor tissue is mainly related to hypoxia. The center of a solid tumor with a volume exceeding 2 mm^3 could not obtain sufficient oxygen and nutrients through diffusion alone, and cells in this region are subject to starvation and a hypoxic microenvironment.[4,5] Tumors constantly adapt to their current harsh living environment and gradually develop blood vessels to ensure sufficient oxygen supply.[6] The angiogenesis of tumor tissue mainly involves two different processes: vasculogenesis and angiogenesis.[7] vasculogenic mimicry (VM) is associated with various tumors, such as melanoma; hepatocellular carcinoma; and breast, gastric, colorectal, prostate, and lung cancers.[8–14] Therefore, it has become an important marker for the evaluation of tumor malignancy. Meanwhile, inhibiting tumors by inhibiting angiogenesis has been proven to be effective and has guided drug research and development.[1,15–19]

However, the *in vitro* evaluation methods for angiogenesis are mainly based on the comprehensive detection of cell budding, proliferation, and migration ability, and the effect of the research object on angiogenesis has only been indirectly discussed.[20–25] Vascular formation and spheroid budding experiments are also widely used to evaluate the angiogenic ability of endothelial cells *in vitro*. The number of branch points that form the lumen network and the total length of the network were used to evaluate the influence of various factors on angiogenesis comprehensively.[26,27] The above evaluation methods are all static observations that feature certain subjectivity and limitation.[28] However, objective scientific evaluation of dynamic analysis of angiogenesis has not been conducted. The present study aimed to develop a highly representative and objective method for the evaluation of angiogenesis and then describe the dynamic process of angiogenesis well.

Therefore, imaging results were analyzed using a live-cell imaging-based code. The continuous dynamic VM (vasculogenic mimicry) process was captured by live-cell imaging technology, and ImageJ and the developed AngiogenesisAnalyzer.ijm (Data S1) and AutoMeasure.ijm (Data S1) were used to digitize the images. The simultaneous development of VM.R (Data S1) could automatically generate the obtained data into pictures to determine a representative, repeatable, and sensitive measurement method that could truly and objectively describe angiogenesis, further promoting the research of cell biology and guiding the development of anti-angiogenesis drugs and clinical diagnosis and treatment.

[1]State Key Laboratory of Medicinal Chemical Biology and College of Pharmacy, Nankai University, Tianjin, China

[2]Lead contact

*Correspondence: liuhuijuanxyz@163.com (H.L.), sunrockmia@hotmail.com (T.S.)

https://doi.org/10.1016/j.isci.2023.106721

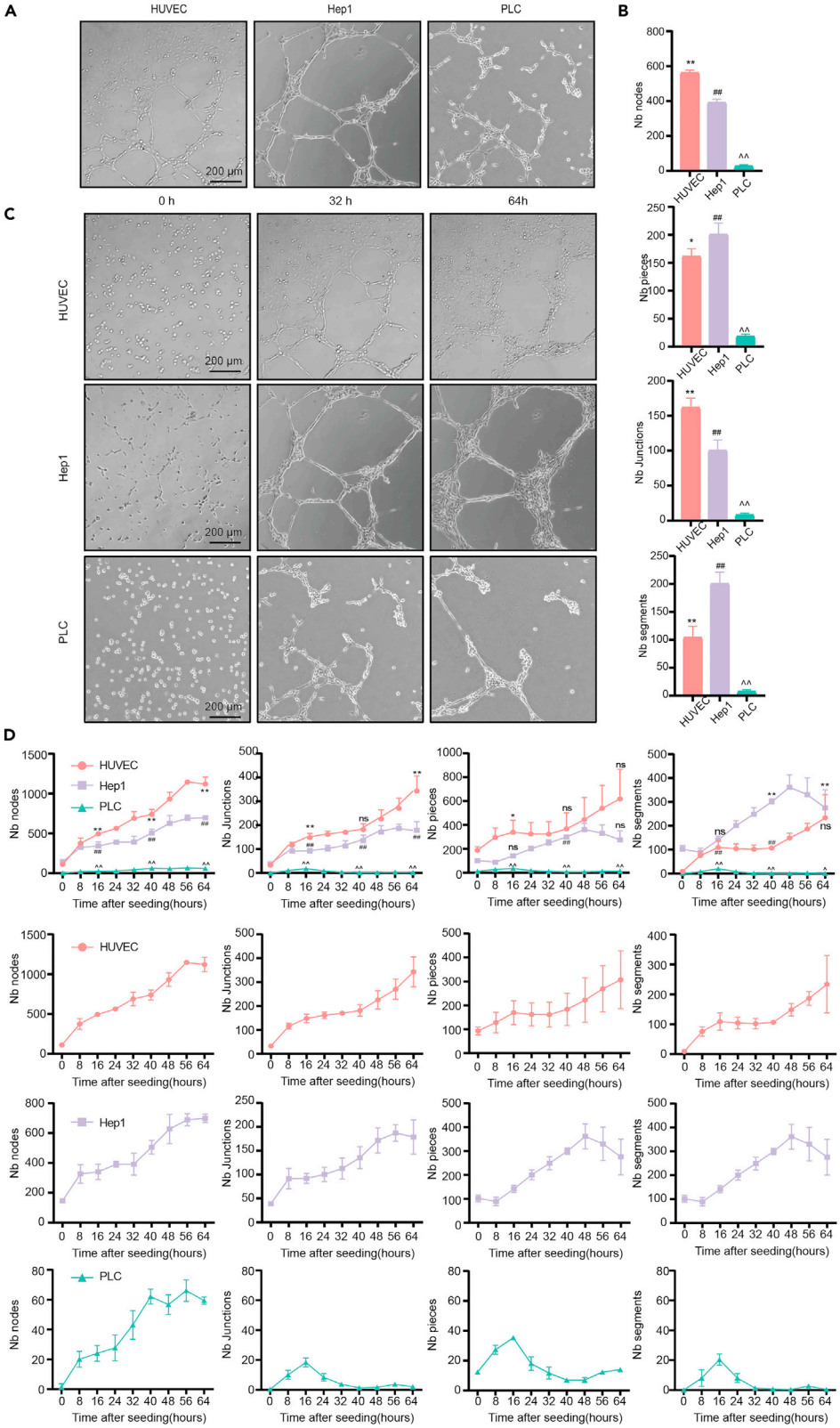
A
HUVEC
Hep1
PLC
200 μm
B
Nb nodes
Nb pieces
Nb Junctions
Nb segments
C
0 h
32 h
64h
D
Time after seeding(hours)

Figure 1. Existing vascular evaluation methods cannot objectively reflect the real situation

(A and B) Representative figures of VM observations and quantitative plots of the four measurement parameters at 24 h in HUVECs, Hep1, and PLC cell lines.

(C and D) Representative plots of VM status of HUVEC, Hep1, and PLC cells at 0, 32, and 64 h and quantitative plots of the four measured parameters at 1 h intervals for the three groups of cells. Quantitative analysis presented as a line graph. All values are presented as mean ± SEM (n = 3), multivariate analysis. Two-way ANOVA (or mixed model) was performed at 16, 40, and 64 h with GraphPad Prism.* represents the difference between HUVEC and Hep1, # represents the difference between Hep1 and PLC, and ^ represents the difference between PLC and HUVEC. Error bars: S.D. Scale: 200 μm
*$p < 0.05$,**$p < 0.01$, ^$p < 0.05$, ^^$p < 0.01$, #$p < 0.05$, ##$p < 0.01$, without significant difference (*ns*).

RESULTS

Different observation time points and measurement standards affect judgment

Vascular endothelial cells (HUVECs) and two liver cancer cell lines, namely, PLC (Primary Liver Carcinoma) (not prone to VM) and Hep1 (prone to VM), were selected for live-cell imaging to observe the VM or angiogenic ability of different cells dynamically. Cell images that were taken at 24 h after cell plating were quantitatively analyzed in accordance with the methods that are widely used in the literature. The main measurement parameters were nodes, junctions, segments, and pieces in the field of view (Figures 1A and 1B). Based on all four parameters, PLC showed the weakest tube-forming ability among the tested cell lines. The parameters node and junction indicated that HUVECs had stronger angiogenic ability than PLC and Hep1. The other two parameters segment and pieces illustrated that Hep1 had stronger VM ability than the other cell lines. This situation led to differences in the results of different measurement parameters and therefore obviously did not objectively and truly demonstrate the angiogenic or VM capabilities of the three different cell lines. It was presumed to only evaluate the cell condition at 24 h and thus could not provide a highly detailed description of angiogenesis during cell growth. Therefore, images at multiple time points of live cell-imaging were analyzed (Figures 1C and 1D). According to the four measurement parameters, HUVECs and Hep1 cells showed relatively stable growth in the early stage. However, the growth of Hep1 cells was slower than that of HUVECs, and Hep1 cells showed a slightly downward trend from 48 h to 64 h. PLC cells demonstrated weak VM ability as a whole, with only a small amount of fluctuations between 0 and 32 h (Figures 1C and S1). The experiment found that short time intervals were associated with high accuracy of the expression of the vascular condition. In addition, the same cell lines presented different trends under different measurement parameters, leading to doubtful objectivity of the traditional vascular evaluation methods. Whether the four measurement parameters could truly reflect the cell state and whether superior measurement parameters were available could be determined at 24 h.

Development of vascular formation analysis code

Live-cell imaging technology was used to continuously observe the vascular formation of cells within 64 h to qualitatively analyze the angiogenic ability and prove that evaluating angiogenesis only at the dynamic level is more objective (Video S1). Moreover, screenshots were taken every 5 min to analyze the image information in accordance with different parameters to quantitatively analyze the tube volume. Two problems needed to be solved urgently: which parameter is scientific and which parameter could be correctly described as pipe performance. Therefore, in accordance with the process of angiogenesis and the characteristics of each stage, a set of AngiogenesisAnalyzer.ijm was developed (Figure S2). It could be used as a plug-in of ImageJ to analyze images and obtain data related to angiogenic capability. Compared with the existing plug-ins, AngiogenesisAnalyzer.ijm could adjust the conventional measurement standards, such as node and junction, to make them more suitable for capturing the accurate changes in different parameters in a short time during the dynamic change process (Table 1). It could analyze 20 data types, thus greatly enriching the measurement criteria. The whole process of angiogenesis is described in detail in all aspects. In addition, the principle of AngiogenesisAnalyzer.ijm is clear, and the operation is simple. In solving the first problem, the following complete experiments were designed on the basis of consistency and sensitivity (Figures 3 and S2–S4, described in detail later). Second, each field of view had 768 images in 64 h. According to AngiogenesisAnalyzer.ijm (Data S1), each image had 20 parameters, so an enterprise had 15,360 data points. Therefore, automatic batch analysis codes AutoMeasure.ijm and VM.R were compiled (Data S1). When AutoMeasure.ijm was used together with AngiogenesisAnalyzer.ijm, it could quickly process thousands of pictures to obtain tens of thousands of data points and automatically recognize picture information to generate tabular output data. VM.R automatically processes the obtained data into a line chart or a bar chart in batches. The original thousands of steps could be simplified into several steps and improve the work efficiency hundreds of times.

Table 1. Definition of measurement parameters

Vectorial element	Short defintion
Node	Pixels with at least three adjacent pixels in the next nine pixels
Extrem	Pixel having only one neighbor
Junction	Groups of nodes forming a bifurcation
master junction	Groups of nodes forming a master bifurcation
Branch	Binary line linked with one junction and one extremity
Branching interval	Size loss of due segment
segment	Binary line linked with two junctions
isol.segment	A binary line connected very close to a connection point and an endpoint
Mesh	Map of the meshes consisting in closed areas surrounded by segments
Piece	Sum of the number of segments, isolated elements, and branches

The specific usage method is as follows: AngiogenesisAnalyzer.ijm is the algorithm part. It is copied to macros under the installation directory of ImageJ (for example, if the ImageJ directory is E: Fiji.app, it is placed into E: Fiji.app macros) for the subsequent batch processing calls. AutoMeasure.ijm is the batch processing part. This code is opened through ImageJ,[29] "run" is clicked to run it, and then the directory where the image is located is selected to confirm. The picture data could be automatically batch processed under the folder. VM.R refers to batch processing. All the data below are from the analysis code.

Meanings of measurement parameters in Angiogenesis Analyzer

The definition rules on node, junction, and extreme are shown in the vessel unit (Figure 2A). The vascular network formed by multiple vascular units also included the measurement parameters of the vascular unit and exhibited the nodes, junctions, and extremes in the vascular network (Figure 2Ba). The vascular network formed by two or more adjacent vascular units had corresponding measurement parameter branches, segments, mesh, and isolated segments (Figures 2Bc–2Be). The process from c–e reflected the growth of blood vessels. The segment indicated by the red arrow was shortening, and the two branches were slowly converging and growing into a segment. The process from e, d, and c could also indicate capillary degeneration with two branches forming through segment disconnection. This process is the reason why numerous measurement parameters changed over time. After the image was analyzed using Angiogenesis Analyzer, the graph formed by the measurement parameters and the picture formed by superimposing the original image and the processed picture were obtained (Figure 2C). An overlay of multiple images was also analyzed using Angiogenesis Analyzer (Figure 2D).

Nb. nodes and Tot. length have good stability and sensitivity for evaluation of cell vascular formation

HUVECs were selected, photographed, and quantitatively analyzed every 5 min over 64 h to reflect the vascular condition objectively and accurately. Twenty measurement parameters were used in three different visual fields of the same well. Given the excessively large amount of data, AutoMeasure.ijm, which is matched with AngiogenesisAnalyzer.ijm, was developed to process images into data and then to process the data into a line chart through VM.R. The figure shows the quantitative analysis of cells every 1 h. The experimental group was divided into three groups to test the consistency and sensitivity of the 20 measurement parameters.

Scientific measurement parameters should have good consistency. By selecting the same cell in different fields of view in the same well plate, the consistency of its living environment must be ensured. Therefore, the measurement parameters that met the requirements should be curves that should perform consistently over time under multiple groups of experiments. Nb. nodes, Nb. extremes, Nb isol.seg., Nb junctions, branching intervals, Tot. branching length, Tot. isol. branch length, Tot. segment length, and Tot. length, Nodes represented by the red arrows and the extremes represented by the purple arrows were changed with different groupings of 2 and 64 h (Figure S2).

In-depth experiments were further conducted on the consistency evaluation, and 20 measurement parameters were analyzed in accordance with the above operations and quantitative analysis of HUVECs in different

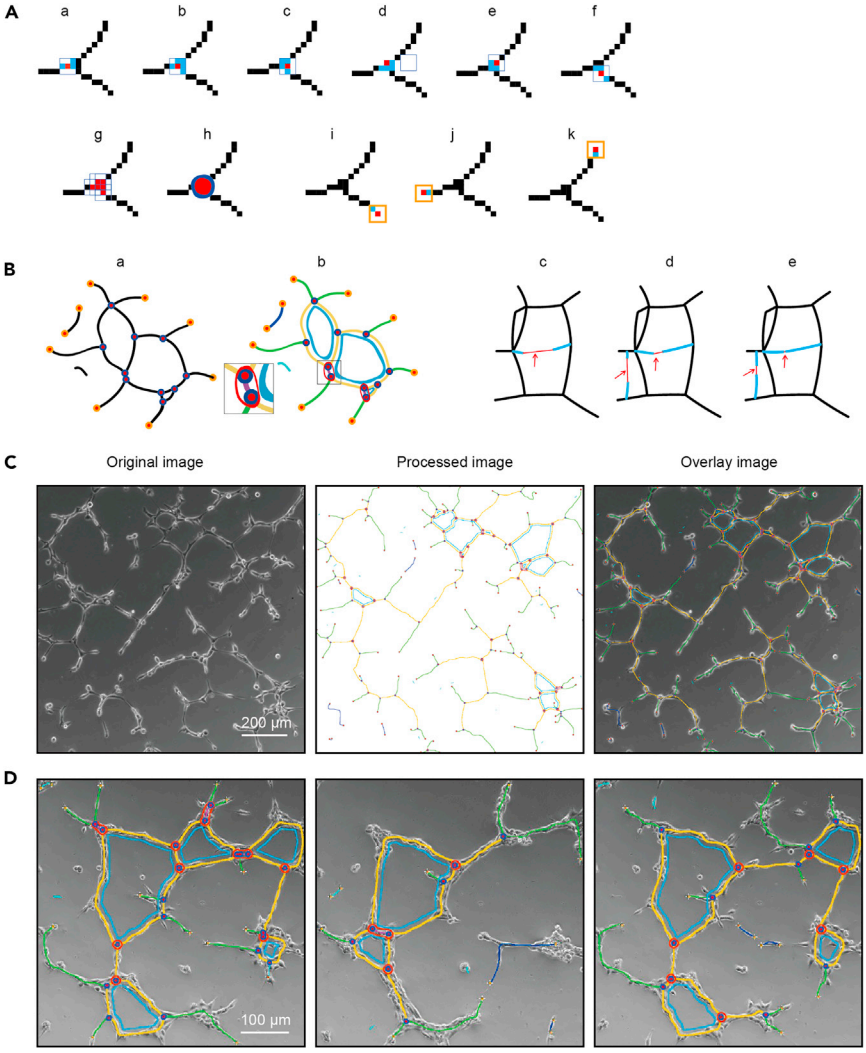

Figure 2. Measurement parameters of blood vessels related to Data S1, Video S1

(A) Three or more pixels exist in the eight pixels around one pixel, which is called a node (abcde). The combination of multiple adjacent nodes to form a circular materialized graph is called a junction (gh). Only one pixel is present in the eight pixels around a pixel, and the circular shape formed with the pixel as the center and the diameter of three pixels is called an extrem (ijk).

(B) A red dot surrounded by a yellow circle represents an extrem, and a red dot surrounded by a dark blue circle represents a junction (a). The line segment formed by the connection of two junctions is called segment (yellow), the line segment formed by a junction and an extrem connection is called branch (green), and the line segment formed by the connection of two extremes is called isolate branch (dark blue). The enclosed area is called mesh (lake blue), the area enclosed by two or more close junctions is called master junction (encircled by red circle), and, in the master junction, the segment formed by the connection of two junctions is called branching (purple). Orginal image, Processed image, and Overlay image.

(C) Overlay images obtained after analysis by Angiogenesis Analyzer. Scale: 200 μm.

(D) Multiple images are overlaid after analysis by Angiogenesis Analyzer. Scale: 100 μm.

wells to further prove the scientific objectivity of the measurement parameters. The same cells in different wells were selected, and nothing was added to the cells in different wells. Therefore, the measurement parameters that met the requirements should also show a relatively consistent curve over time under multiple groups of experiments. The six measurement parameters with good consistency are Nb. nodes, Nb. extreme, Nb. junctions, Nb. meshes, Nb. pieces, and Tot. length. Nodes represented by the red arrows and the extremes represented by the purple arrows were changed with different groupings of 2 and 64 h (Figure S3).

Scientific measurement parameters should have good sensitivity, in addition to consistency. Different concentrations of VEGFA (Vascular Endothelial Growth Factor A) were added to HUVECs in the logarithmic growth phase to promote angiogenesis by different degrees. Given that drugs were added to different groups of cells, the measurement parameters that met the requirements should be relatively different in multiple groups of experiments. Nb. nodes, Mean mesh size, Nb. branches, Nb. extremes, Nb. master junctions, Nb. master segments, Tot. length, and other 16 measurement parameters showed superior sensitivity in different dosing cell groups. The changes in nodes in different groups at 2 and 64 h were represented by red arrows, and those in extreme were represented by purple arrows (Figures S2–S4). Therefore, the same cells in different fields of view in the same well and the same cells in different wells were selected to verify the consistency. Moreover, sensitivity was verified by adding different doses of VEGFA to the same cells. The measurement parameters that met the requirements for each screening were summarized. The two measurement parameters Nb. nodes and Tot. length that met the requirements presented in Figures S2–S4 were selected as the measurement parameters for judging the ability of angiogenesis or vessel mimicry (red box in Figure 3).

Nb. nodes, Tot. length, and time have mathematical relationship in the process of cell formation

HUVECs, Hep1 cells, and PLC cells in the logarithmic growth phase were subjected to blood vessel detection. The analysis revealed that the three kinds of cells had great differences in their angiogenic abilities. Within 64 h, the three cell lines exhibited curves in the form of the measurement parameter Tot. length that resembled a normal distribution or a quartic function. HUVECs showed considerably faster increases than Hep1 and PLC cells over 0–10 h. However, Hep1 cells were more persistent than the other cells, and PLC cells had weak overall vascularization (Figure 4A). The curves for the measurement standard Nb. nodes shown by the three cell lines were similar to linear functions. The vascularization ability of HUVECs was significantly stronger than that of the other cell lines. Hep1 cells showed small increases before and after 30 h, and PLC cells had weak overall vascularization ability (Figure 4B). Therefore, through specific analysis of the blood vessel formation ability of these three kinds of cells, their inherent scientific problems could be further explored. The following conclusions could be drawn:

Quantitative analysis was performed after taking images of HUVECs, Hep1 cells, and PLC cells at 1 h intervals and by analyzing Nb. nodes and Tot. length (Figures 4A and 4B). The Tot. length of the three cells rose and then fell to 0. The Tot. length of HUVECs rose rapidly from 0 to 15 h with a maximum value of over 20,000. The Tot. length of Hep1 cells had a smaller increase than that of HUVECs and peaked at only approximately 15,000 at 40 h. PLC cells had worse VM ability than the two other cell lines, and their Tot. length value decreased to 0 at 40 h. The Nb. nodes of all three cells increased and then leveled off. On the basis of this measurement standard, HUVECs showed stronger ability than the other two cell lines, with the maximum value of more than 1,200. The Nb. nodes of Hep1 cells rose slowly and finally stabilized at approximately 700, and those of PLC cells rose most slowly and reached the maximum value of less than 200. The curves of different cells undergoing subdivision under different standards were rich in information. Seven subdivision standards, such as duration and peak, were statistically analyzed (Figures 4C and 4D). The results of the excavated information were analyzed and interpreted (Table 2). MATLAB was used to simulate the time-varying curves of the three cells (Figure 4E) for interpretation with increased intuitiveness (Table 3).

Sorafenib and LPS (Lipopolysaccharides) could affect the mathematical relationship of Tot. length and Nb. nodes with time

Sorafenib and LPS stimulating factors were added to Hep1 cells in the logarithmic growth phase, and the cell status was observed and recorded every 1 h. Within 64 h, the cell images at every 8 h were selected as representative images (Figures 5A and S5). The statistics of the Tot. length and Nb. nodes of different groups of cells showed that different drugs affected not only the peaks of cellular vascular mimetic production but also the occurrence time of the highest peaks of cellular VM and the decay rates of Tot. length and Nb. nodes (Figures 5B and 5D). Statistical analysis was performed on seven subdivisions, including duration and peak (Figures 5C and 5E). The results were analyzed and interpreted for the mined information (Table 4). After data analysis, with Tot. length as the evaluation criterion, no difference was found in the duration of vascular mimesis in the three different methods. Compared with the normal group, the sorafenib group grew slowly at the first 30 h to 2,706, which was 10,688 smaller than the peak of the normal group, and then maintained at the highest level. Meanwhile, the LPS group grew rapidly in the first 20 h to

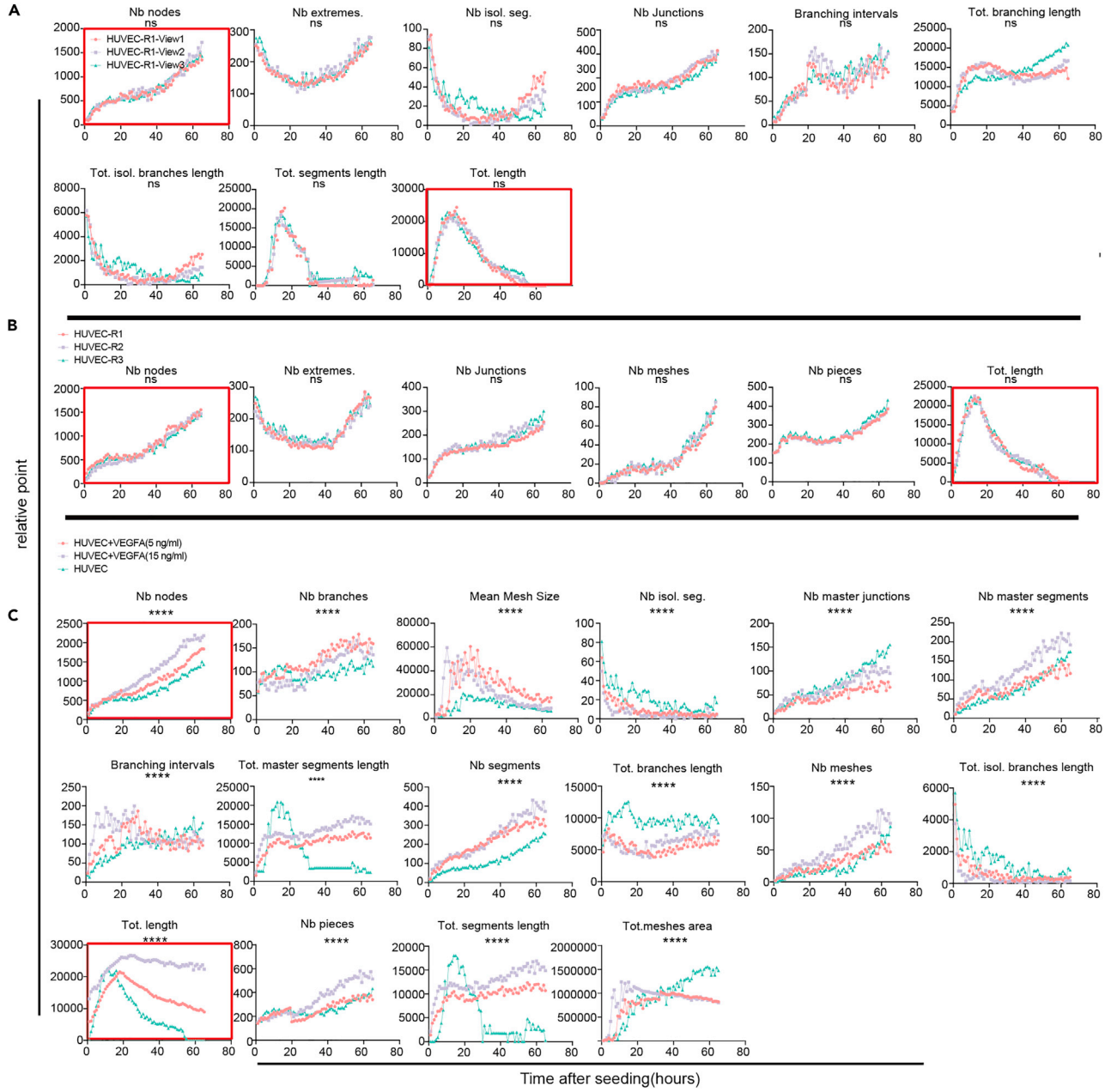

Figure 3. Summary of measurement parameter screening

(A) HUVEC cells in different fields of view in the same well; the consistency of 20 measurement parameters was detected, and 9 measurement parameters were in line with the standard.

(B) The consistency of HUVEC cells in different wells was tested for 20 measurement parameters, and the 6 measurement parameters met the standard.

(C) After HUVEC cells were subjected to different treatments, the sensitivity of 20 measurement parameters was tested, and 16 measurement parameters found to be in line with the standard. (A–C) In the red box, Nb nodes and Tot. length satisfied all the conditions. They met the requirements presented in Figures S2–S4 at the same time and were selected as the measurement parameters for judging the ability of angiogenesis or vessel mimicry. All values represent mean ± SEM (n = 3), One-way ANOVA (and nonparametric or mixed), GraphPad Prism. Error bars: S.D. *p < 0.05, **p < 0.01, no significant difference (*ns*).

19,741 and then quickly eliminated. By using Nb. nodes as the evaluation criterion, the Hep1 cells treated with three different methods did not differ in the duration of VM. Compared with the normal group, the sorafenib group also showed a slow growth in the first 30 h of 269, smaller than the peak of the normal

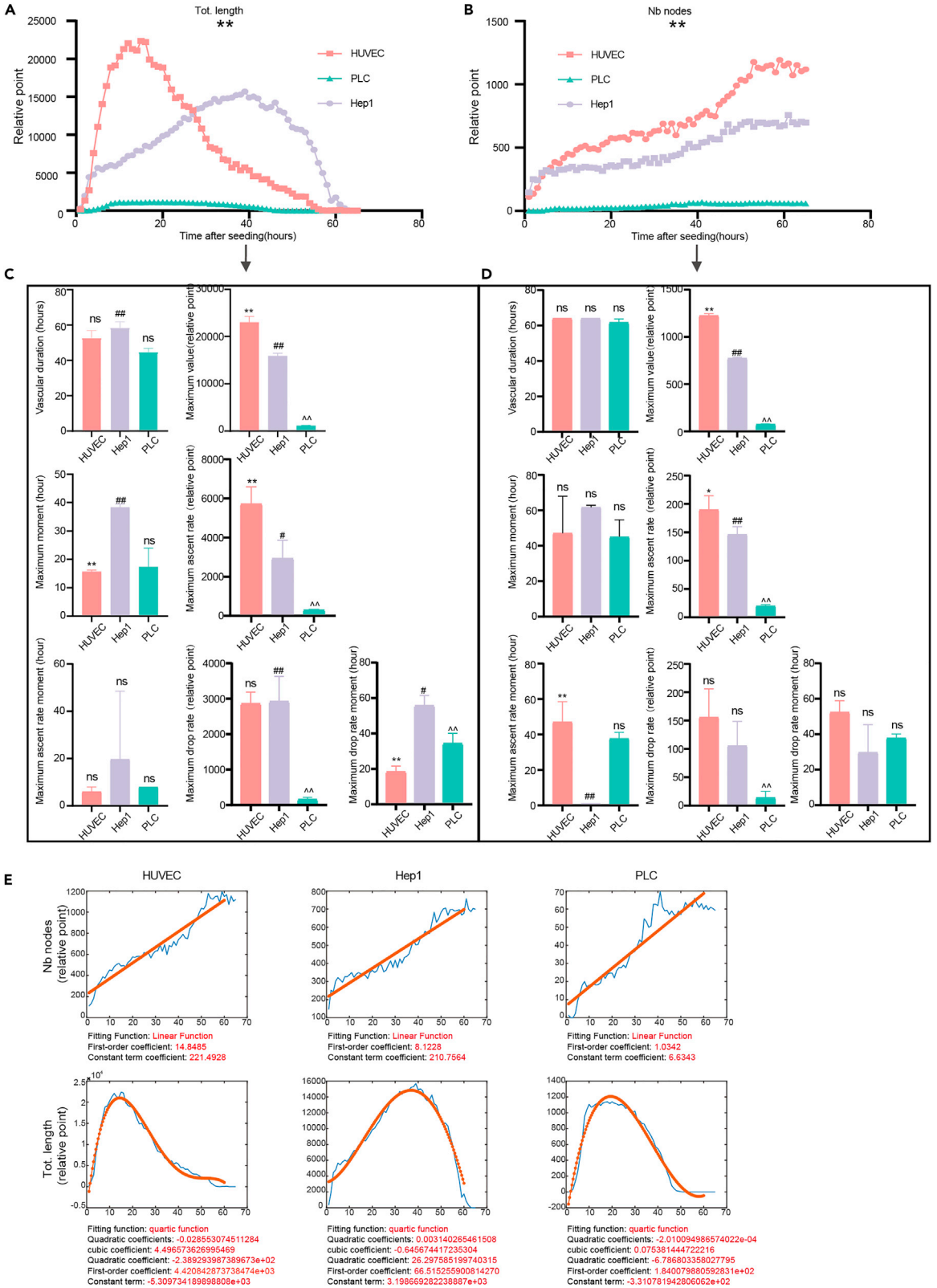
A
Tot. length
**
Relative point
Time after seeding(hours)
HUVEC
PLC
Hep1
B
Nb nodes
**
Relative point
Time after seeding(hours)
HUVEC
PLC
Hep1
C
D
Vascular duration (hours)
Maximum value(relative point)
Maximum moment (hour)
Maximum ascent rate (relative point)
Maximum ascent rate moment (hour)
Maximum drop rate (relative point)
Maximum drop rate moment (hour)
ns
##
**
^^
#
HUVEC
Hep1
PLC
E
HUVEC
Hep1
PLC
Nb nodes (relative point)
Fitting Function: Linear Function
First-order coefficient: 14.8485
Constant term coefficient: 221.4928
Fitting Function: Linear Function
First-order coefficient: 8.1228
Constant term coefficient: 210.7564
Fitting Function: Linear Function
First-order coefficient: 1.0342
Constant term coefficient: 6.6343
Tot. length (relative point)
Fitting function: quartic function
Quadratic coefficients: -0.028553074511284
cubic coefficient: 4.496573626995469
Quadratic coefficient: -2.3892939873896 73e+02
First-order coefficient: 4.420842873738474e+03
Constant term: -5.309734189898808e+03
Fitting function: quartic function
Quadratic coefficients: 0.003140265461508
cubic coefficient: -0.645674417235304
Quadratic coefficient: 26.297585199740315
First-order coefficient: 66.515255900814270
Constant term: 3.198669282238887e+03
Fitting function: quartic function
Quadratic coefficients: -2.0100949865 74022e-04
cubic coefficient: 0.075381444722216
Quadratic coefficient: -6.786803358027795
First-order coefficient: 1.840079880592831e+02
Constant term: -3.310781942806062e+02

Figure 4. Application of Tot. length and Nb nodes in different cell lines

(A and B) Quantitative analysis of the two measurement parameters in accordance with the angiogenesis of HUVECs and Hep1 and PLC cells over 64 h at 1 h intervals. All values represent mean ± SEM (n = 3), One-way ANOVA (and nonparametric or mixed), GraphPad Prism. *p < 0.05, **p < 0.01, no significant difference (*ns*).

(C and D) In-depth quantitative analysis of Tot. length and Nb node data according to the angiogenesis of HUVECs, Hep1, and PLC cells at 1 h intervals over 64 h. Presented as a histogram.

(E) Formulas obtained for HUVECs and Hep1 and PLC cells simulated and analyzed by using MATLAB. All values represent mean ± SEM (n = 3), two-way ANOVA (or mixed model) for multivariate analysis, GraphPad Prism.* represents the difference between HUVEC and Hep1, # represents the difference between Hep1 and PLC, and ^ represents the difference between PLC and HUVEC. Error bars: S.D. *p < 0.05,**p < 0.01, ^p < 0.05, ^^p < 0.01, #p < 0.05, ##p < 0.01, without significant difference (*ns*).

group, and then slowly eliminated. The LPS group showed rapid growth in the first 20 h of 1000 and then slowly eliminated.

Independent variables Nb. nodes maximum value, Tot. length maximum value, and Tot. length maximum drop rate were used during the whole process of vascularization to better describe the vascularization capability in different groupings by Tot. length and Nb. nodes (Figure S6A) *in vitro*, with VEGF (Vascular Endothelial Growth Factor) relative as a standard (Figure S6B). The function equation y (VEGF relative content) = 0.002998× Nb. nodes maximum value + 0.00007983× Tot. length maximum value −0.001345× Tot. length maximum drop rate −0.422670 was simulated with VEGF relative content *in vitro*. The functional equation y (MVD value) = 0.026133 × Nb. nodes maximum value +0.001880 × Tot. length maximum value −0.017971 × Tot. length maximum drop rate +0.773271 was simulated with MVD value *in vivo*. Micrangum arc as the standard Figures S6C and S6D). The relative amount of VEGF in *in vitro* vascularization was inferred from the Nb. nodes maximum value, Tot. length maximum value, and Tot. length maximum drop rate during the entire process of vascularization. The MVD value for *in vivo* vascularization was also inferred.

Table 2. Specific analysis of blood vessel formation ability of different cell lines

	Tot. length	Nb nodes
Duration	The duration of Tot. length was not different between Hep1 and HUVEC but was approximately 15 h longer than PLC.	Hep1, HUVEC, and PLC nodes all had longer duration, no significant difference.
Maximum value	The maximum value of the total vessel length of HUVEC was the largest, which was 7174 higher than Hep1 and 21886 higher than PLC. There are significant differences among the three.	The maximum number of HUVEC nodes was the largest, which was 452 higher than Hep1 and 1151 higher than PLC. There were significant differences.
Maximum time	Both HUVEC and PLC reached the peak of total vessel length earlier, and there was no difference; both reached the peak 20 h earlier than Hep1.	There was no difference between the three.
maximum acceleration	The maximum increase rate of Tot. length of HUVEC was 1.95 times that of Hep1 and 18.99 times that of PLC.	The maximum increase rate of HUVEC was the largest, 44 larger than Hep1 and 170 larger than PLC.
Time of maximum acceleration	Hep1, HUVEC, and PLC all reached the maximum rate of ascent moment was earlier, with no difference.	HUVEC and PLC reached the maximum rate of ascent moment is later, more than 30 h later than Hep1. There was no difference between the three.
Maximum deceleration	The maximum drop of ascent of Hep1 and HUVEC were both larger and had no difference, and both were more than 18 times the elimination rate of PLC.	Hep1 and HUVEC had larger maximum deceleration, and there was no difference. HUVEC was more than 5 times that of PLC, and there was no difference between Hep1 and PLC.
Time of maximum deceleration	HUVEC reaches maximum rate of ascent moment was earlier, 10 h earlier than PLC and 30 h earlier than Hep1.	Hep1, HUVEC, and PLC all reached the maximum rate of ascent moment was later, and there was no difference.

Table 3. Vascular formation simulation formula

Measurement parameter	HUVEC	Hep1	PLC
Tot. length	$Y = 14.8485X + 221.4928$	$Y = 8.1228X + 210.7564$	$Y = 1.0342X + 6.6343$
Nb nodes	$Y = -0.029X^4 + 4.497X^3 - 2.389X^2 + 4.421X - 5.310$	$Y = 0.003X^4 - 0.646X^3 + 26.298X^2 + 66.515X + 3.199$	$Y = -2.010X^4 + 0.075X^3 - 6.787X^2 + 1.840X - 3.311$

Y: the ability of Vascular formation X; the time.

The XYZ values were given, resulting in a unique point on the three-dimensional image that corresponds to a color that is either the relative content of VEGF or the MVD value (Figure S6E). Subsequently, the simulated function was validated to demonstrate the accuracy of the modification, as specifically expanded later.

Vitexicarpin shows potential antivascular effect

Vitexicarpin, geniopicroside (GPS), and salidroside (SAL) were added to the wild-type (WT) Hep1 in the logarithmic growth stage, the cell condition was observed every 1 h, and the representative plot was selected every 8 h (Figures 6A and S7). Through the statistics of Tot. length and Nb. nodes of different groups of cells, different treatment groups were found to affect not only the peaks of cellular vascular mimetic production but also the occurrence of the highest peaks of cellular VM and the growth rate of Tot. length and Nb. nodes (Figures 6B and 6D). Statistical analysis was performed on seven subdivisions, including duration and peak (Figures 6C and 6E). The results of the mined information analysis and interpretation are shown in Table 5. According to the data analysis, with Tot. length as the evaluation criterion, the Hep1 cells treated by three different methods were 5–10 h shorter than the normal group in VM. Compared with the normal group, the GPS group grew rapidly in the first 20 h to 12,577, which was about 3151 smaller than the peak of the normal group, and then quickly eliminated. Meanwhile, the vitexicarpin and SAL groups grew slowly in the first 20 h to about 2,724 and 4,877, respectively, and then slowly eliminated. With Nb. nodes as the evaluation criterion, the Hep1 cells treated by three different methods had a shorter vascular mimic duration than the normal group by 10–15 h. Compared with the normal group, the GPS group grew rapidly in the first 20 h, growing to 715, which was similar to the peak of the normal group, and then maintained rapid elimination. Meanwhile, the vitexicarpin and SAL groups grew slowly in the first 20 h to about 305 and 582, respectively, and then rapidly eliminated (Table 5).

Vitexicarpin inhibits tumor VM and malignant evolution *in vitro*

Vitexicarpin inhibited the effect of VM in vitro, and it was confirmed to have the strongest effect on the basis of Tot. length and Nb. nodes. The effect of vitexicarpin on the growth of Hep1 cells *in vitro* was further studied. The Hep1 cells in the logarithmic growth phase were selected, and the experimental group was treated with vitexicarpin. The clone formation experiment showed that the proliferation ability of the treatment group had doubled compared with that of the control group (Figure 7A). The results of migration and invasion were similar to those of VM. In the experimental group treated with vitexicarpin, the migration and invasion ability decreased to one-fourth (Figures 7B and 7C). In the scratch experiment, photographs were taken every 12 h to verify the effect of vitexicarpin on the wound-healing ability of tumor cells. The experimental group showed a weaker ability to promote tumor cell wound healing within 24 h than the control group. Moreover, the healing speed of the experimental group was nearly 35% slower than that of the control group (Figure 7D). Meanwhile, the effect of vitexicarpin on the expression of VM-related proteins was verified through immunofluorescence experiment and western blot analysis, and the expression of MMP2, VEGFR1, and VEGFR2 proteins in the vitexicarpin-treated experimental group significantly decreased compared with that in the control group (Figures 7E and 7F). The Nb. nodes and Tot. length were presented by cells in different dosing groups, concluding that vitexin has greater potential ability to inhibit VM. For verification that the function of Figure S6E was correct, the statistically obtained Nb. nodes maximum value, Tot. length maximum value, and Tot. length maximum drop rate were treated as independent variables by simulating the function of VEFG relative content. The relative expression of VEGF in the supernatant of vitexicarpin-induced Hep1 cells was found to be 0.3466667, and that measured by ELISA was 0.342861977, without significant difference (Figure S6F). Furthermore, the function simulated could well speculate the amount of cellular VEGF expression *in vitro* by Nb. nodes and Tot. length. This study provides support for the subsequent prediction of this formula in terms of its capacity for VM.

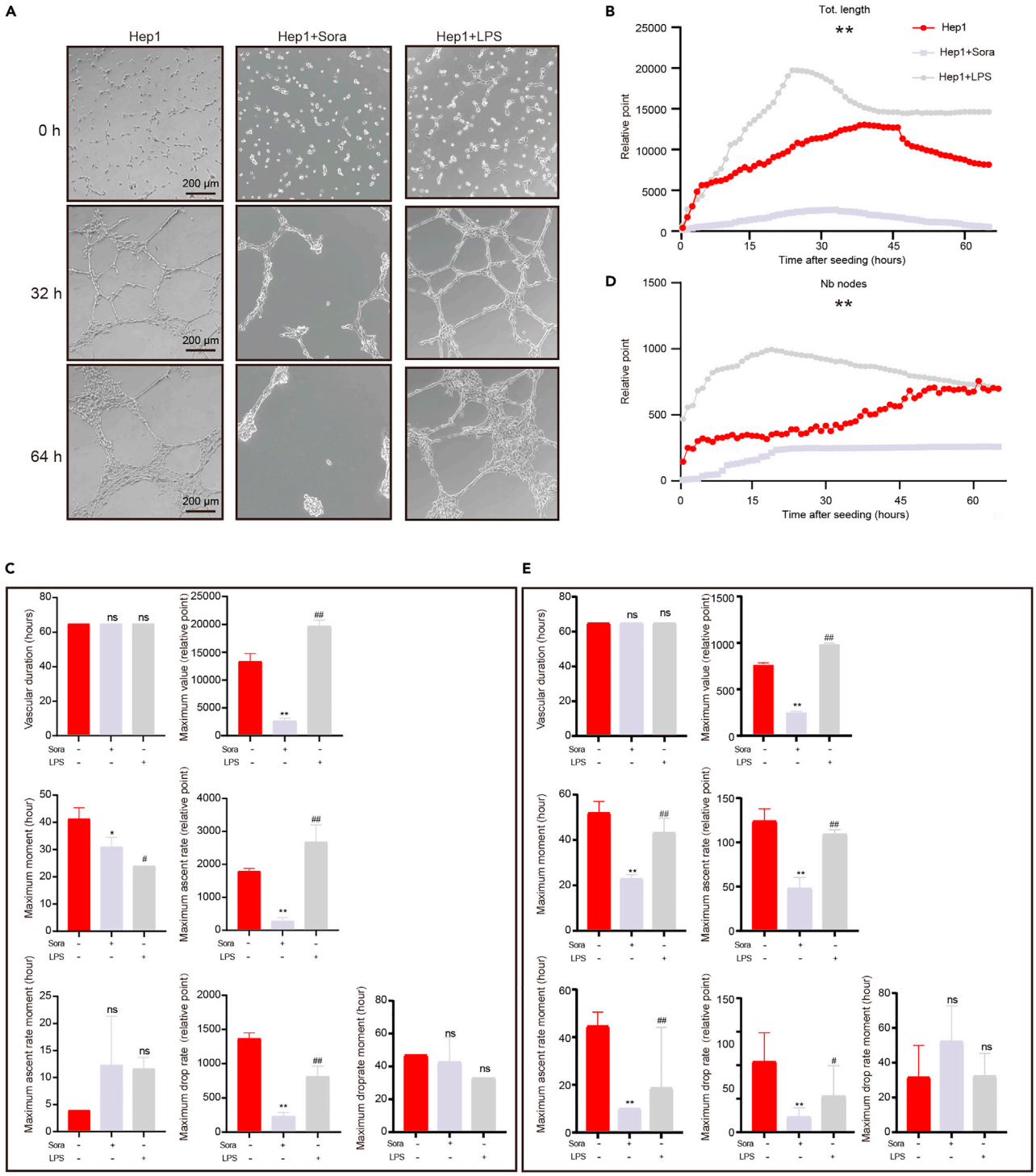

Figure 5. Tubeformation of Hep1 after sorafenib and LPS treatment as reflected by Tot. length and Nb nodes

(A) Representative plots of VM in three groups under different treatments and wild-type (WT) Hep1.

(B and D) Quantitative maps of VM status based on Tot. length and Nb nodes in different groups of Hep1 observed over at 0, 32, and 64 h. Quantitative analysis of the number of microvessels, presented in the form of a line graph. All values represent mean ± SEM (n = 3), one-way ANOVA (and nonparametric or mixed), GraphPad Prism.

Figure 5. *Continued*

(C and E) Specific quantitative analysis of vascular mimicry status in three groups of differently treated Hep1 at 1-h intervals for 64 h. Presented as a histogram. All values represent mean ± SEM (n = 3), two-way ANOVA (or mixed model) for multivariate analysis, GraphPad Prism. * represents the difference between Sora group and Hep1 group, and # represents the difference between Hep1 group and LPS group. Error bars: S.D. Scale: 200 μm*$p < 0.05$,**$p < 0.01$, $^{\#}p < 0.05$, $^{\#\#}p < 0.01$, without significant difference (*ns*).

Vitexicarpin inhibits tumor VM and malignant evolution *in vivo*

The tumor model was established through subcutaneous injection of Hep1 cells in the logarithmic growth phase into 6-week-old nude mice. At 5 days post-injection, vitexicalpin was injected into the tumor every 3 days for 2 weeks. The state of the mice was observed and recorded, and the mice were euthanized when the maximum tumor volume increased by approximately 1,500 mm^3. When the mouse model was established, the overall state of the mice was observed and recorded. Within 14 days, the tumor volume increased nearly twice (Figures 8A and 8B), and the body weight decreased by approximately 12% in mice intratumorally injected with vitexicarpin relative to that of the control mice. Moreover, the mouse state score significantly increased (Figures 8C and 8D). The immunohistochemistry analysis of tumor tissue demonstrated that in the treatment group, KI67, which is related to malignancy, significantly decreased, and VEGFR1 and VEGFR2, which are related to VM, significantly decreased. CD31 (Platelet endothelial cell adhesion molecule-1) /periodic acid Schiff (PAS) double-positive staining and PAS single-positive signaling also indicated that the treated group had fewer microvessels than the control group. The red arrow in the small frame represented the PAS^+ signal, and the black arrow represented the $CD31^+/PAS^+$ signal (Figures 8E and 8F). For verification that the function of Figure S6E was correct, the statistically obtained Nb. nodes maximum value, Tot. length maximum value, and Tot. length maximum drop rate were treated as independent variables by simulating the function of MVD values *in vivo*. The MVD of tumor tissue slices after intratumoral injection by vitexicarpin was found to be 8.6666667, and the average value of MVD in tumor tissue intratumorally injected with vitexin was 8.970227, without significant difference (Figure S6G).

Table 4. Specific analysis of blood vessel formation ability of Hep1 cells after different treatments

	Tot. length	Nb. nodes
Duration	No difference could be found among the sorafenib, LPS, and control groups.	No difference could be found among the sorafenib, LPS, and control groups.
Maximum value	The maximum value of the LPS group exceeded that of the normal and sorafenib groups by 2706 and 10,688, respectively.	The LPS group formed the most nodes, and the score was 248 higher than that of the normal group, while the normal group was 464 higher than the sorafenib group.
Maximum time	The LPS group reached the maximum time the earliest, 17 h faster than the normal group, whereas the normal group was 10 h slower than the sorafenib group.	No difference was found between the sorafenib group and the normal group in reaching the maximum time, which was 20 h faster than the LPS group.
Maximum acceleration	The maximum rate of ascent in the LPS group was 1.50 times that of the normal group, while the normal group was 6.21 times faster than the sorafenib group.	The maximum rate of ascent in the LPS group was 3.78 times that in the normal group, and the normal group was 2.58 times faster than the sorafenib group.
Time of maximum acceleration	The normal, sorafenib, and LPS groups reached the maximum rate of ascent moment early, without difference.	No difference could be observed between the LPS group and the normal group in reaching the maximum rate of ascent moment, which was 26 h faster than the sorafenib group.
Maximum deceleration	The maximum drop of ascent in the normal group was 1.67 times that of the LPS group and 5.88 times that of the sorafenib group.	The maximum deceleration in the normal group was 1.94 times that of the LPS group and 2.35 times that of the sorafenib group.
Time of maximum deceleration	The time to reach the maximum rate of ascent moment in the normal, sorafenib, and LPS groups was late, without difference.	The time to reach the maximum rate of ascent moment in the normal, sorafenib, and LPS groups was late, without difference.

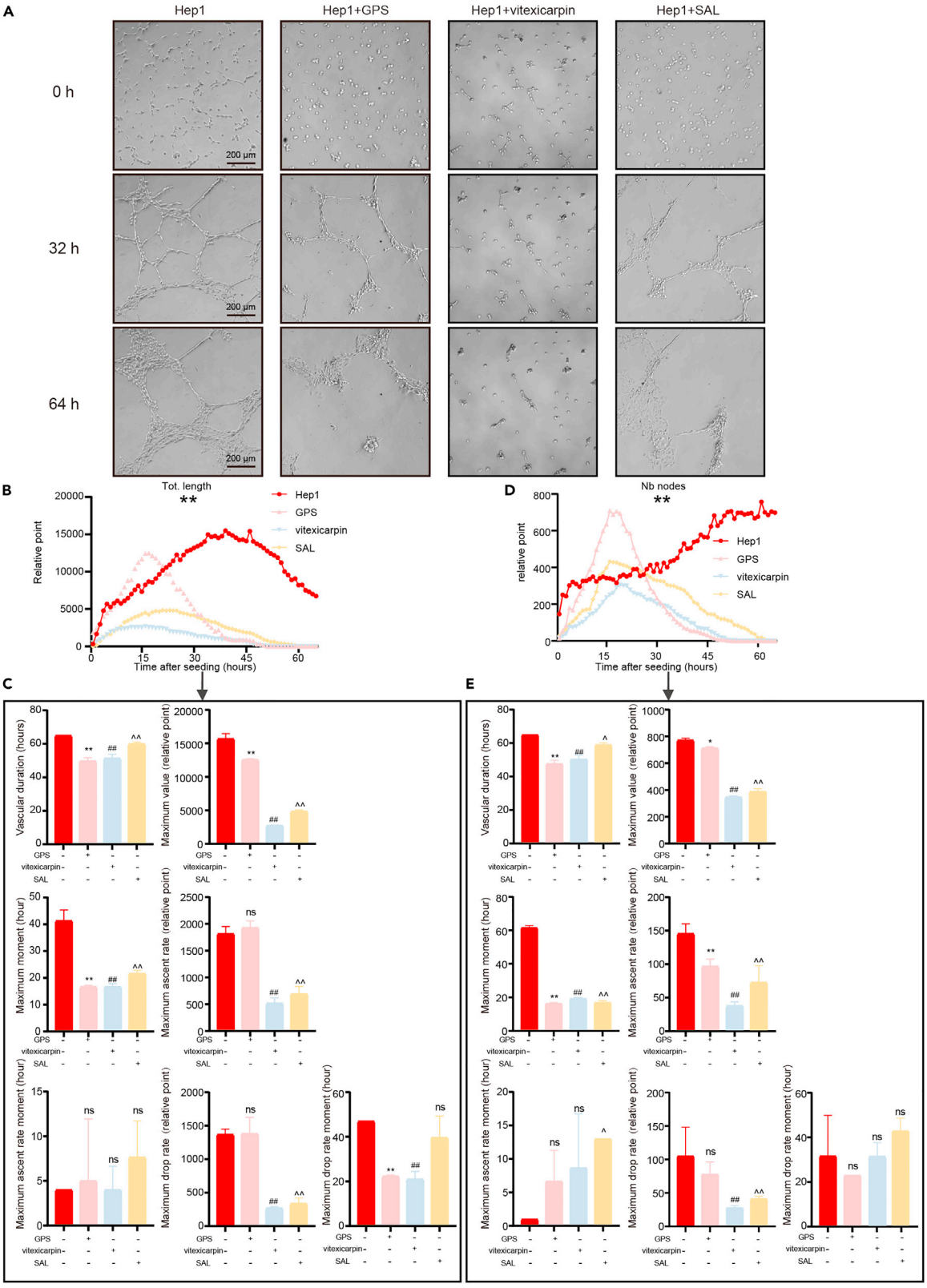
A
Hep1
Hep1+GPS
Hep1+vitexicarpin
Hep1+SAL
0 h
32 h
64 h
200 μm
B
Tot. length
**
Relative point
Time after seeding (hours)
Hep1
GPS
vitexicarpin
SAL
D
Nb nodes
**
relative point
Time after seeding (hours)
C
E
Vascular duration (hours)
Maximum value (relative point)
Maximum moment (hour)
Maximum ascent rate (relative point)
Maximum ascent rate moment (hour)
Maximum drop rate (relative point)
Maximum drop rate moment (hour)
GPS
vitexicarpin
SAL
ns

Figure 6. Vascular formation of Hep1 after GPS, vitexicarpin, and SAL treatment as reflected by Tot. length and Nb nodes

(A) Representative images of VM observed in the four groups of Hep1 at 0, 32, and 64 h after different treatments.

(B–D) Quantitative analysis of vessels in different groups of Hep1 observed over 64 h at 1 h intervals with Tot. length and Nb nodes. Presented as a line graph. All values represent mean ± SEM (n = 3), one-way ANOVA (and nonparametric or mixed), GraphPad Prism.

(C–E) Vessel-specific quantification of four groups of differently treated WT Hep1 at 1 h intervals over 64 h. Presented as a histogram. All values represent mean ± SEM (n = 3), two-way ANOVA (or mixed model) for multivariate analysis, GraphPad Prism. * represents the difference between GPS group and Hep1 group, # represents the difference between Hep1 group and vitexicarpin group, and ^ represents the difference between Hep1 group and SAL group. Error bars: S.D. Scale: 200 μm *$p < 0.05$,**$p < 0.01$, ^$p < 0.05$, ^^$p < 0.01$, #$p < 0.05$, ##$p < 0.01$, without significant difference (*ns*).

DISCUSSION

A growing number of studies have confirmed that dysregulation of angiogenesis is closely related to physiological and pathological processes. The objective and scientific descriptions given by *in vitro* assays for cell vascular formation provide the basis for guiding drug screening and cell biology research.

Tot. length well describes the process of intussusceptive (splitting) angiogenesis, which is the formation of cellular tubular structures and their extension to each cell to form a network. Nb. nodes correspond to the formation of cell nodes in the initial process of sprouting angiogenesis. The proposed method could help identify the aspects of vascular formation that are affected by different cells or drugs. Existing antivascular drug screening methods are mainly based on molecular docking and functional verification. The method is more direct and convincing in directly judging the specific links that affect angiogenesis than the traditional method. By exploiting this difference, new monomers, such as GPS, vitexicarpin, and SAL, were discovered. A dynamic process could provide additional valuable information. The effect of different stimuli on the angiogenic ability of a certain cell line is also reflected in different forms by different measurement parameters. The same measurement parameter may reflect different forms of inhibition or activation. For example, the effect of a certain inhibitor on the inhibition of angiogenesis or VM could be reflected by quantitative changes, and the highest peaks of some angiogenesis and growth curves may have differences. This effect could also be reflected by the changes in the time axis, and some angiogenesis growth

Table 5. Specific analysis of Hep1 vascular mimicry capacity after different treatments

	Tot. length	Nb. nodes
Duration	The duration of the vitexicarpin, GPS, and SAL groups was 5–10 h shorter than that of the normal group.	The duration of the vitexicarpin, GPS, and SAL groups was 10–15 h shorter than that of the normal group.
Maximum value	The maximum values of the GPS, vitexicarpin, and SAL groups could reach about 12,577, 2727, and 4877, respectively, whereas that of the normal group was as high as about 15728.	The maximum values of the GPS, vitexicarpin, and SAL groups could reach about 714, 305, and 582, respectively, whereas that of the normal group was as high as about 773.
Maximum time	The maximum time of the vitexicarpin, GPS, and SAL groups was about 24 h later than that of the normal group.	The maximum time of the vitexicarpin, GPS, and SAL group was about 30 h later than that of the normal group.
Maximum acceleration	The maximum rate of ascent in the GPS group was similar to that in the normal group, while the normal group was about three times as fast as the vitexicarpin and SAL groups.	The maximum rate of ascent in the normal group was 1.5 times that of the GPS group, about 4.52 times that of the vitexicarpin group, and about 2.32 times that of the SAL group.
Time of maximum acceleration	The normal, GPS, vitexicarpin, and SAL groups reached the maximum rate of ascent moment early, without difference.	No difference could be found among the normal, GPS, and vitexicarpin groups, which was 5–10 h earlier than the SAL group.
Maximum deceleration	The maximum deceleration in the GPS group was similar to that in the normal group, while the normal group was about five times as fast as the vitexicarpin and SAL groups.	The maximum deceleration in the GPS group was similar to that in the normal group, while the normal group was about three times as fast as the vitexicarpin and SAL groups.
Time of maximum deceleration	The normal and SAL groups reached the maximum rate of ascent moment later than the GPS and vitexicarpin groups.	The time to reach the maximum rate of node elimination was earlier in the normal, sorafenib, and VEGFA groups, without difference.

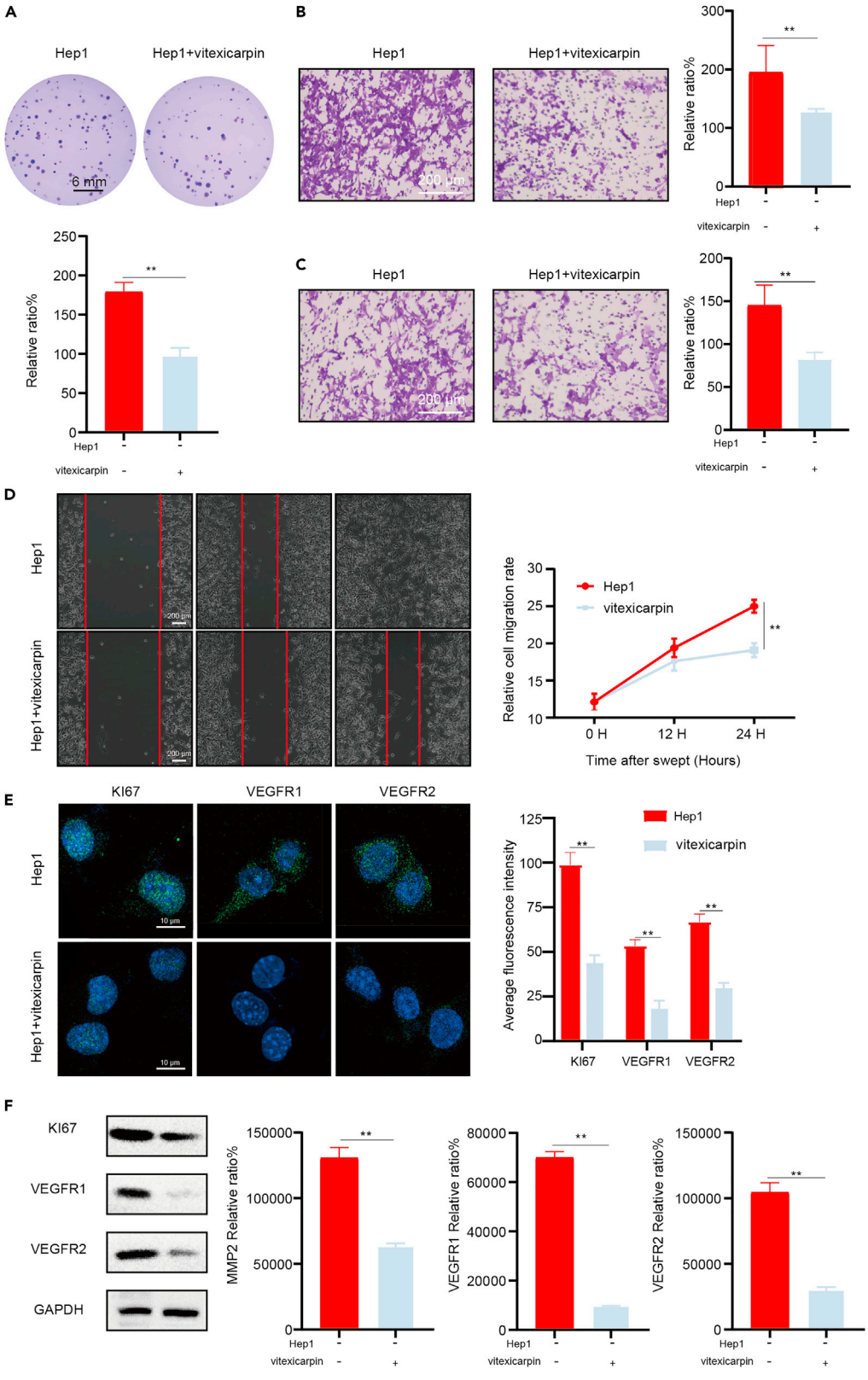
A
Hep1
Hep1+vitexicarpin
6 mm
Relative ratio%
Hep1
vitexicarpin
B
Hep1
Hep1+vitexicarpin
200 μm
Relative ratio%
C
Hep1
Hep1+vitexicarpin
200 μm
Relative ratio%
D
Hep1
Hep1+vitexicarpin
Relative cell migration rate
Hep1
vitexicarpin
0 H
12 H
24 H
Time after swept (Hours)
E
KI67
VEGFR1
VEGFR2
Hep1
Hep1+vitexicarpin
10 μm
Average fluorescence intensity
Hep1
vitexicarpin
KI67
VEGFR1
VEGFR2
F
KI67
VEGFR1
VEGFR2
GAPDH
MMP2 Relative ratio%
VEGFR1 Relative ratio%
VEGFR2 Relative ratio%
Hep1
vitexicarpin

Figure 7. Vitexicarpin inhibits the occurrence and development of tumor cells *in vitro*

(A) Representative graphs of single-cell clone formation in the control and vitexicarpin-treated experimental groups and quantitative statistical analysis after 8 days, presented as a histogram.Scale: 6 mm.

(B and C) Quantitative statistical analysis of migration and invasion experiments, presented as a histogram.Scale: 200 μm.

(D) Representative graphs of scratch experiments at 0, 12, and 24 h. Red lines mark the edges of the scratches. Relative gap length quantification was performed every 12 h, presented as a line graph.Scale: 200 μm.

(E) Immunofluorescence experiments on the control and experimental groups.Scale: 10 μm.

(F) Western blot analysis of MMP2, VEGFR1, VEGFR2, and other proteins in the experimental and control groups and quantitative evaluation of the Western blot results. Presented as a histogram (left). All data represent mean ± SEM (n = 3); one-way analysis of variance (ANOVA). Error bars: S.D.*$p < 0.05$, **$p < 0.01$, not significantly different (*ns*).

curves may have different peak times. The total length of the blood vessel or the duration of the number of nodes, the highest peak, the growth rate, the elimination rate, and the appearance of the highest peak could be used as evaluation criteria for vascular formation ability. This information could not be observed through a static process. Therefore, on the basis of the dynamic imaging of live cells and code analysis, cell biological issues could be studied and drug development, clinical diagnosis, and treatment could be guided.

Tot. length and Nb. nodes could be fitted with corresponding functions. Vascular conditions could be assessed by analyzing the constant terms of different powers. For example, under Nb. nodes, the blood vessel formation curve satisfied the equation $y = Ax + B$. The sign of A indicates whether the blood vessel is growing or shrinking. Size describes the rate of growth or shrinkage. B represents the number of nodes formed at the beginning. In addition, with Nb. nodes maximum value, Tot. length maximum value, and Tot. length maximum drop rate as independent variables, a ternary function was fitted to speculate the desired expression of VEGF and the MVD value. By analyzing these data, relevant information could be explored in depth.

The changes in blood vessels in cell lines under different treatments could be described scientifically and objectively in accordance with the new proposed method. Given the massive amount of data processed, three sets of codes were included to batch process the images into data and then processed into line charts to complete the data analysis. The method will be open sourced to those who need it. More importantly, the traditional static observation of many biological behaviors may not be accurate and objective at this stage. Developing more software and scripts to study the dynamic change process may help understand the nature of things more scientifically.

Limitations of the study

Our current research focuses on the correlation analysis of angiogenesis, which is a single phenomenon, and cannot effectively interpret other key biological phenomena of physiology and pathology. At the same time, the current work has not further revealed the principle at the mechanism level.

ETHICS DECLARATIONS

Animal experiments were performed in accordance with the National Institutes of Health guidelines for the use of animals. All experimental protocols were approved by the laboratory Animal Care and Use Committee of Nankai University. Document number: 2022-sydwll-000590.

STAR★METHODS

Detailed methods are provided in the online version of this paper and include the following:

- KEY RESOURCES TABLE
- RESOURCE AVAILABILITY
  - Lead contact
  - Materials availability
  - Data and code availability
- EXPERIMENTAL MODEL AND SUBJECT DETAILS
  - Xenograft tumor model
- CELL CULTURE AND TREATMENTS
- METHOD DETAILS

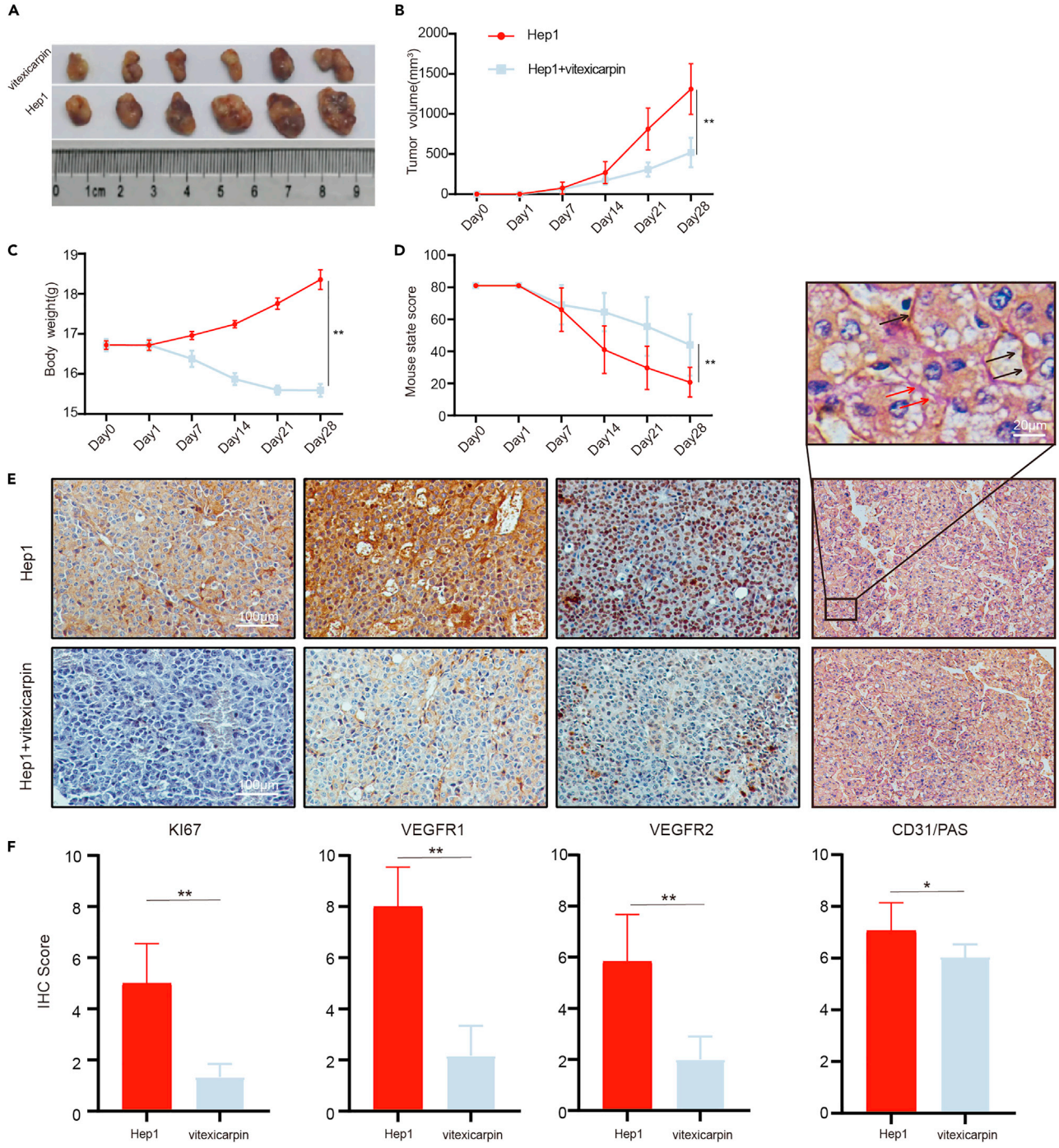

Figure 8. Intratumoral injection of vitexicarpin into tumor-bearing mice inhibited tumors

(A) Representative tumor images of normal Hep1 tumor-bearing mice (n = 6) and tumor-bearing mice after intratumoral injection of vitexicarpin.

(B–D) Statistical analysis of tumor size, body weight, and mouse state score indicators of the two groups of mice within 14 days, presented in the form of a line graph. All values represent mean ± SEM (n = 6); unpaired Student's t-test; *p < 0.05, **p < 0.01, not significantly different (ns).

(E and F) Immunohistochemical analysis of tumor tissue, representative images and scoring, scoring criteria: positivity (1–3 points), and area (1–3 points). The picture in the lower right corner is a 100× tumor tissue section immunohistochemistry picture, the red arrow in the small frame represents the $CD31^{-}/PAS^{+}$ signal, and the black arrow represents the $CD31^{+}/PAS^{+}$signal. Presented in the form of a histogram. All values represent mean ± SEM (n = 6); unpaired Student's t-test. Error bars: S.D. *p < 0.05, **p < 0.01, not significantly different (*ns*).Scale: 100 μm and 20 μm.

- Immunohistochemical and HE staining
- Tumor microvascular density (MVD) detection
- Wound-healing assay
- Colony formation assay
- Cell migration assay and invasion assay
- Immunofluorescence staining
- Western blot analysis
- VM in vitro
- ELISA

- QUANTIFICATION AND STATISTICAL ANALYSIS

SUPPLEMENTAL INFORMATION

Supplemental information can be found online at https://doi.org/10.1016/j.isci.2023.106721.

ACKNOWLEDGMENTS

This work was supported by the National Natural Science Foundation of China (Grant nos. 82073205, 81872374, and 81871972), the Fundamental Research Funds for the Central Universities, Nankai University, Tianjin Science Fund for Distinguished Young Scholars (21JCZDJC00930 and 19JCJQJC63200), the National Youth Talent Support code (2020), Hundred Young Academic Leaders code of Nankai University, and China Postdoctoral Science Foundation (No. 2021M701778).

AUTHOR CONTRIBUTIONS

Zhi-Yang Li carried out experiments, analyzed data, drafted the manuscript, and edited figures. Yu-Jie Sun, Zhuang-Zhuang Feng, and Bijia Cui carried out experiments and analyzed data. Heng Zhang, Yi-Nan Li, Jing-Xia Han, and Hui-Juan Liu provided technical support. Tao Sun conceived experiments, edited the manuscript, and secured funding. All authors had final approval of the submitted and published versions of the manuscript.

DECLARATION OF INTERESTS

The authors declare no competing interests.

INCLUSION AND DIVERSITY

One or more of the authors of this paper self-identifies as an underrepresented ethnic minority in their field of research or within their geographical location. One or more of the authors of this paper received support from a program designed to increase minority representation in their field of research. While citing references scientifically relevant for this work, we also actively worked to promote gender balance in our reference list. We support inclusive, diverse, and equitable conduct of research.

Received: November 9, 2022
Revised: March 2, 2023
Accepted: April 19, 2023
Published: April 23, 2023

REFERENCES

1. Goel, S., Duda, D.G., Xu, L., Munn, L.L., Boucher, Y., Fukumura, D., and Jain, R.K. (2011). Normalization of the vasculature for treatment of cancer and other diseases. Physiol. Rev. *91*, 1071–1121. https://doi.org/10.1152/physrev.00038.2010.

2. Jiang, X., Wang, J., Deng, X., Xiong, F., Zhang, S., Gong, Z., Li, X., Cao, K., Deng, H., He, Y., et al. (2020). The role of microenvironment in tumor angiogenesis. J. Exp. Clin. Cancer Res. *39*, 204. https://doi.org/10.1186/s13046-020-01709-5.

3. Wang, X., Freire Valls, A., Schermann, G., Shen, Y., Moya, I.M., Castro, L., Urban, S., Solecki, G.M., Winkler, F., Riedemann, L., et al. (2017). YAP/TAZ orchestrate VEGF signaling during developmental angiogenesis. Dev. Cell *42*, 462–478.e7. https://doi.org/10.1016/j.devcel.2017.08.002.

4. Lee, P., Chandel, N.S., and Simon, M.C. (2020). Cellular adaptation to hypoxia through hypoxia inducible factors and beyond. Nat. Rev. Mol. Cell Biol. *21*, 268–283. https://doi.org/10.1038/s41580-020-0227-y.

5. Mao, X.G., Xue, X.Y., Wang, L., Zhang, X., Yan, M., Tu, Y.Y., Lin, W., Jiang, X.F., Ren, H.G., Zhang, W., and Song, S.J. (2013). CDH5 is specifically activated in glioblastoma stemlike cells and contributes to vasculogenic mimicry induced by hypoxia. Neuro Oncol. *15*, 865–879. https://doi.org/10.1093/neuonc/not029.

6. Delgado-Bellido, D., Serrano-Saenz, S., Fernández-Cortés, M., and Oliver, F.J. (2017). Vasculogenic mimicry signaling revisited: focus on non-vascular VE-cadherin. Mol.

Cancer *16*, 65. https://doi.org/10.1186/s12943-017-0631-x.

7. Luo, Q., Wang, J., Zhao, W., Peng, Z., Liu, X., Li, B., Zhang, H., Shan, B., Zhang, C., and Duan, C. (2020). Vasculogenic mimicry in carcinogenesis and clinical applications. J. Hematol. Oncol. *13*, 19. https://doi.org/10.1186/s13045-020-00858-6.

8. Bai, X.L., Zhang, Q., Ye, L.Y., Liang, F., Sun, X., Chen, Y., Hu, Q.D., Fu, Q.H., Su, W., Chen, Z., et al. (2015). Myocyte enhancer factor 2C regulation of hepatocellular carcinoma via vascular endothelial growth factor and Wnt/β-catenin signaling. Oncogene *34*, 4089–4097. https://doi.org/10.1038/onc.2014.337.

9. Camorani, S., Crescenzi, E., Gramanzini, M., Fedele, M., Zannetti, A., and Cerchia, L. (2017). Aptamer-mediated impairment of EGFR-integrin αvβ3 complex inhibits vasculogenic mimicry and growth of triple-negative breast cancers. Sci. Rep. *7*, 46659. https://doi.org/10.1038/srep46659.

10. Li, W., Zong, S., Shi, Q., Li, H., Xu, J., and Hou, F. (2016). Hypoxia-induced vasculogenic mimicry formation in human colorectal cancer cells: involvement of HIF-1a, Claudin-4, and E-cadherin and Vimentin. Sci. Rep. *6*, 37534. https://doi.org/10.1038/srep37534.

11. Li, Y., Wu, Z., Yuan, J., Sun, L., Lin, L., Huang, N., Bin, J., Liao, Y., and Liao, W. (2017). Long non-coding RNA MALAT1 promotes gastric cancer tumorigenicity and metastasis by regulating vasculogenic mimicry and angiogenesis. Cancer Lett. *395*, 31–44. https://doi.org/10.1016/j.canlet.2017.02.035.

12. Meng, J., Chen, S., Lei, Y.Y., Han, J.X., Zhong, W.L., Wang, X.R., Liu, Y.R., Gao, W.F., Zhang, Q., Tan, Q., et al. (2019). Hsp90β promotes aggressive vasculogenic mimicry via epithelial-mesenchymal transition in hepatocellular carcinoma. Oncogene *38*, 228–243. https://doi.org/10.1038/s41388-018-0428-4.

13. Schnegg, C.I., Yang, M.H., Ghosh, S.K., and Hsu, M.Y. (2015). Induction of vasculogenic mimicry overrides VEGF-A silencing and enriches stem-like cancer cells in melanoma. Cancer Res. *75*, 1682–1690. https://doi.org/10.1158/0008-5472.Can-14-1855.

14. Wu, S., Yu, L., Wang, D., Zhou, L., Cheng, Z., Chai, D., Ma, L., and Tao, Y. (2012). Aberrant expression of CD133 in non-small cell lung cancer and its relationship to vasculogenic mimicry. BMC Cancer *12*, 535. https://doi.org/10.1186/1471-2407-12-535.

15. Jayson, G.C., Kerbel, R., Ellis, L.M., and Harris, A.L. (2016). Antiangiogenic therapy in oncology: current status and future directions. Lancet *388*, 518–529. https://doi.org/10.1016/s0140-6736(15)01088-0.

16. Tie, J., and Desai, J. (2012). Antiangiogenic therapies targeting the vascular endothelia growth factor signaling system. Crit. Rev. Oncog. *17*, 51–67. https://doi.org/10.1615/critrevoncog.v17.i1.50.

17. Willett, C.G., Boucher, Y., di Tomaso, E., Duda, D.G., Munn, L.L., Tong, R.T., Chung, D.C., Sahani, D.V., Kalva, S.P., Kozin, S.V., et al. (2004). Direct evidence that the VEGF-specific antibody bevacizumab has antivascular effects in human rectal cancer. Nat. Med. *10*, 145–147. https://doi.org/10.1038/nm988.

18. Yang, J.P., Liao, Y.D., Mai, D.M., Xie, P., Qiang, Y.Y., Zheng, L.S., Wang, M.Y., Mei, Y., Meng, D.F., Xu, L., et al. (2016). Tumor vasculogenic mimicry predicts poor prognosis in cancer patients: a meta-analysis. Angiogenesis *19*, 191–200. https://doi.org/10.1007/s10456-016-9500-2.

19. Yuan, F., Chen, Y., Dellian, M., Safabakhsh, N., Ferrara, N., and Jain, R.K. (1996). Time-dependent vascular regression and permeability changes in established human tumor xenografts induced by an anti-vascular endothelial growth factor/vascular permeability factor antibody. Proc. Natl. Acad. Sci. USA *93*, 14765–14770. https://doi.org/10.1073/pnas.93.25.14765.

20. Das, A., Huang, G.X., Bonkowski, M.S., Longchamp, A., Li, C., Schultz, M.B., Kim, L.J., Osborne, B., Joshi, S., Lu, Y., et al. (2018). Impairment of an endothelial NAD(+)-H(2)S signaling network is a reversible cause of vascular aging. Cell *173*, 74–89.e20. https://doi.org/10.1016/j.cell.2018.02.008.

21. De Bock, K., Georgiadou, M., Schoors, S., Kuchnio, A., Wong, B.W., Cantelmo, A.R., Quaegebeur, A., Ghesquière, B., Cauwenberghs, S., Eelen, G., et al. (2013). Role of PFKFB3-driven glycolysis in vessel sprouting. Cell *154*, 651–663. https://doi.org/10.1016/j.cell.2013.06.037.

22. Longchamp, A., Mirabella, T., Arduini, A., MacArthur, M.R., Das, A., Treviño-Villarreal, J.H., Hine, C., Ben-Sahra, I., Knudsen, N.H., Brace, L.E., et al. (2018). Amino acid restriction triggers angiogenesis via GCN2/ATF4 regulation of VEGF and H(2)S production. Cell *173*, 117–129.e14. https://doi.org/10.1016/j.cell.2018.03.001.

23. Schoors, S., Bruning, U., Missiaen, R., Queiroz, K.C., Borgers, G., Elia, I., Zecchin, A., Cantelmo, A.R., Christen, S., Goveia, J., et al. (2015). Fatty acid carbon is essential for dNTP synthesis in endothelial cells. Nature *520*, 192–197. https://doi.org/10.1038/nature14362.

24. Wang, X., Abraham, S., McKenzie, J.A.G., Jeffs, N., Swire, M., Tripathi, V.B., Luhmann, U.F.O., Lange, C.A.K., Zhai, Z., Arthur, H.M., et al. (2013). LRG1 promotes angiogenesis by modulating endothelial TGF-β signalling. Nature *499*, 306–311. https://doi.org/10.1038/nature12345.

25. Yu, P., Wilhelm, K., Dubrac, A., Tung, J.K., Alves, T.C., Fang, J.S., Xie, Y., Zhu, J., Chen, Z., De Smet, F., et al. (2017). FGF-dependent metabolic control of vascular development. Nature *545*, 224–228. https://doi.org/10.1038/nature22322.

26. Arnaoutova, I., and Kleinman, H.K. (2010). In vitro angiogenesis: endothelial cell tube formation on gelled basement membrane extract. Nat. Protoc. *5*, 628–635. https://doi.org/10.1038/nprot.2010.6.

27. Xin, H., Zhong, C., Nudleman, E., and Ferrara, N. (2016). Evidence for pro-angiogenic functions of VEGF-Ax. Cell *167*, 275–284.e6. https://doi.org/10.1016/j.cell.2016.08.054.

28. Udan, R.S., Culver, J.C., and Dickinson, M.E. (2013). Understanding vascular development. Wiley Interdiscip. Rev. Dev. Biol. *2*, 327–346. https://doi.org/10.1002/wdev.91.

29. Schindelin, J., Arganda-Carreras, I., Frise, E., Kaynig, V., Longair, M., Pietzsch, T., Preibisch, S., Rueden, C., Saalfeld, S., Schmid, B., et al. (2012). Fiji: an open-source platform for biological-image analysis. Nat. Methods *9*, 676–682. https://doi.org/10.1038/nmeth.2019.

STAR★METHODS

KEY RESOURCES TABLE

REAGENT or RESOURCE	SOURCE	IDENTIFIER
Antibodies		
KI67	Proteintech	27309-1-AP (Proteintech Cat# 27309-1-AP; RRID:AB_2756525)
VEGFR1	Affnity	AF6204 (Affinity Biosciences Cat# AF6204; RRID:AB_2835085)
VEGFR2	Affnity	AF6281 (Affinity Biosciences Cat# AF6281; RRID:AB_2835132)
GAPDH	Affinity	AF7021 (Affinity Biosciences Cat# AF7021; RRID:AB_2839421)
CD31	Proteintech	KHC0022 (proteintech Cat# KHC0022)
Chemicals, peptides, and recombinant proteins		
Sorafenib	Macklin	Cat# 284461-73-0
VEGFA	Proteintech	Cat# AG13500
Geniopicroside	Acmec	Cat# G21690
Vitexincarpin	N/A	Cat# 3681-93-4
Salidroside	N/A	Cat# 10338-51-9
Periodic Acid Schiff (PAS) Stain Kit, with Hematoxylin	Solarbio	Cat# G1281
Lipopolysaccharide	Sigma-Aldrich	Cat# L3129-10 MG
Critical commercial assays		
Mouse VEGF ELISA KIT	SHANGHAI TONGWEI BIOTECHNOLOGY CO.,LTD	Cat# TW011232
Deposited data		
AngiogenesisAnalyzer.ijm	This paper	mendely data https://doi.org/10.17632/xw7wvvz936.1
Auto Measure.ijm	This paper	mendely data https://doi.org/10.17632/xw7wvvz936.1
VM.R	This paper	mendely data https://doi.org/10.17632/xw7wvvz936.1
Experimental models: Cell lines		
HUVEC	KeyGen Biotech (Nanjing, China)	N/A
Hep1	KeyGen Biotech (Nanjing, China)	KG064
PLC	KeyGen Biotech (Nanjing, China)	KG068
Experimental models: Organisms/strains		
Mouse: Male BALB/c nude	vitalriver	N/A
Software and algorithms		
ImageJ	Schneider et al.[29]	https://imagej.net/
GraphPad Prism (version 8.0.0)	GraphPad Software	www.graphpad.com
SPSS software (version 25.0)	SPSS Inc.	https://www.ibm.com/support/pages/downloading-ibm-spss-statistics-25
MATLAB R2021a	MathWorks, Inc.	https://mathworks.com/

RESOURCE AVAILABILITY

Lead contact

Further information and requests for code and resources should be directed to and will be fulfilled by the lead contact, Tao Sun (sunrockmia@hotmail.com).

Materials availability

This study did not generate new unique reagents.

Data and code availability

- All data reported in this paper will be shared by the lead contact upon request.
- All original code has been deposited at Mendely Data and is publicly available as of the date of publication. DOIs are listed in the key resources table.
- Any additional information required to reanalyse the data reported in this work is available from the lead contact upon reasonable request.

EXPERIMENTAL MODEL AND SUBJECT DETAILS

Xenograft tumor model

Male BALB/c nude mice aged 4–6 weeks were used in the experiments. According to institutional guidelines, all animals were maintained in a specific pathogen-free animal care facility. Each BALB/c nude mouse was subcutaneously injected with approximately 1×10^6 cells. Tumor diameters were serially measured using a digital caliper every 7 days. Tumor volumes were calculated using the following equation: length × width^2/2. On day 28, the mice were euthanized. Tumor tissues were collected, fixed with 10% formalin, and embedded in paraffin. Animal experiments were performed in accordance with the National Institutes of health guidelines for the use of animals. All experimental protocols were approved by the laboratory animal care and use Committee of Nankai University. Document number: 2022-sydwll-000590.

CELL CULTURE AND TREATMENTS

HUVEC, Hep1, PLC was purchased from ATCC. HUVEC were cultured in endothelial cell medium (ECM, ScienCell) containing 5% fetal bovine serum (FBS, cat. No. 0025), 1% endothelial growth additive (ECGs, cat. No. 1052) and 1% penicillin Streptomycin Solution (PS, cat. No. 0503). Hep1, PLC were cultured in Dulbecco's modified eagle's medium (DMEM, keygen biotech) supplemented with 10% FBS (Thermo Fisher Scientific) And 1% penicillin Streptomycin (hyclone) solution. HUVEC, Hep1, PLC were performed cell culture in 5% CO^2 atmosphere at 37°C.Hep1 cells were seeded in normal Petri dishes, cultured under the above normal culture conditions, and induced by VEGFA. The culture concentrations were 5 ng/mL and 15 ng/mL. The culture medium were changed every three days.Hep1 cells were seeded in a normal culture dish, cultured under the above normal culture conditions, and induced by geniopicroside (GPS), vitexicalpin and salidroside(SAL). The culture concentration was 50 μM, 30 μM and 50 μM.The culture medium were changed every three days.

METHOD DETAILS

Immunohistochemical and HE staining

The mouse tissues were incubated with xylene for deparaffinization and ethanol with decreased concentrations for rehydration. Afterward, 3% hydrogen peroxide was applied to block the endogenous peroxidase activity. The microwave antigen retrieval technique was utilized for antigen retrieval. After blocking was performed, the samples were incubated with the primary antibodies at 4°C overnight. The secondary antibody was subsequently added using an HRP-polymer antimouse/rabbit IHC Kit (Maixin Biotech) at room temperature for 1 h. Finally, sections were developed in DAB solution (Gene Tech) under microscopic observation and counterstained with hematoxylin. The scoring of expression was performed according to both of the ratio and intensity of positive-stained cells: 0–5% scored 0; 6–35% scored 1; 36–70% scored 2; and more than 70% scored 3. In addition, The sections were directly counterstained with hematoxylin or subjected to PAS staining first followed byhematoxylin staining (CD31-PAS staining). The sections were dehydrated, cleared, and placed under coverslips after the reaction. The sections were then examined using light microscope.

The sections were stained with HE staining kit (Solarbio), dewaxed with xylene, treated with graded ethanol, and then washed with tap water. The sections were stained with hematoxylin for 9 min and eosin for 2 min at room temperature. After staining, the sections were dehydrated, sealed, and observed by HE staining with a microscope.

Tumor microvascular density (MVD) detection

The microvessel density (MVD) was evaluated by CD31 immunohistochemistry staining. The entire section was scanned at low magnification (100×) to identify four hot spots. MVD was calculated as the average count of microvessel in the four hot spots at high magnification.

Wound-healing assay

The scratch experiment was performed in a 24-well plate, After the cells are adhered to the plate, the scratch experiment is performed. A straight scratch was created in the center of each well by using a micropipette tip. Cell migration was assessed by measuring the cell movement within the scratch in the well. Scratches were photographed at the beginning of the experiment and after 24 h, 48 h.

Colony formation assay

Colony formation was performed in a 6-well plate. Totally 1×10^3 cells were seeded per dish and cultured for 14 days. Colonies were fixed in 4% paraformaldehyde for 20 min and stained with crystal violet for 7 min at room temperature. The number of colonies was counted by ImageJ.

Cell migration assay and invasion assay

The migrative ability of the cells was determined using a transwell assay. For migration assays, add 2×10^4 cells in 200 μL of serum-free medium to the upper chamber. Then, add 800 μL of medium containing 10% FBS to the bottom chamber. After 24 h of culture, the cells on the lower surface of the filter were fixed with 4% paraformaldehyde fixative (Solarbio), and then the invasive cells were counted with crystal violet staining.

The invasive ability of the cells was determined using a transwell assay. For invasion assays, add 2×10^4 cells in 200 μL of serum-free medium to the upper chamber coated with Matrigel (San Jose, CA, USA). Then, add 800 μL of medium containing 10% FBS to the bottom chamber. After 24 h of culture, the cells on the lower surface of the filter were fixed with 4% paraformaldehyde fixative (Solarbio), and then the invasive cells were counted with crystal violet staining.

Immunofluorescence staining

Cells (5×10^5) were seeded and cultured in 24-well culture plates. The experimental group were treated for 48 h. Then these cells were fixed with 4% paraformaldehyde for 30 min.After washing with filtered PBS, the cells were blocked with 5% BSA for 1 h. Subsequently, samples were incubated with primary antibody(KI67, VEGFR1, VEGFR2) at 4°C overnight. The next day, cells were incubated with Alexa Fluor 647-labeled Goat Anti-Rabbit IgG antibodies at room temperature for 1 h.Then DAPI (Beyotime) was used for nuclei staining. Finally, the images were acquired using a Zeiss lsm800 confocal microscope.

Western blot analysis

Cells were washed with PBS and lysed in ice-cold lysis buffer with protease Inhibitor Cocktail (Sigma) on ice for 30 min. Centrifuge at 4°C 12000 rpm for 10 min,the supernatant was taken and the protein concentration was measured by BCA method, stored in −20°C. Samples were separated through electrophoresis and transferred onto PVDF membranes (Millipore). The membranes were blocked for 2 h, then incubated with primary antibody against KI67, VEGFR1, VEGFR2, GAPDH at 4°C overnight. The next day,samples incubated with a goat anti-rabbit IgG secondary antibody (Beyotime) for 2 h at room temperature. Protein expression was assessed using an enhanced chemiluminescent substrate (Affinity) and exposed to a chemiluminescent film(ChemiScope 6000, CLIX).

VM in vitro

Matrigel (BD Biosciences) was thawed at 4°C, and 200 μL of Matrigel was rapidly added to each well of a 24-well plate, allowed to solidify for 1 h at room temperature, and placed at 37°C in a humidified 5% CO^2 incubator for 30 min. The cells were dissociated by trypsinization, washed in PBS and re-suspended in serum-free medium. Cells were seeded with serum-free medium at a density of 3×10^5 cells per well in the matrigel-coated wells and incubated at 37°C for more than 64 h. Photos of cells were taken under the Living cell microscope (Nikon, Japan) at regular intervals.Numbers of VM tube structures in three random fields were counted.

ELISA

The cells were seeded in 6-well plates and incubated in serum-free medium for 24 h. The conditioned medium was collected, and the concentration of VEGF was quantified using VEGF ELISA kits (SHANGHAI TONGWEI BIOTECHNOLOGY CO.,LTD, Shanghai, China) according to the manufacturer's instructions. All experiments were performed in triplicate.

QUANTIFICATION AND STATISTICAL ANALYSIS

GraphPad Prism (version number 8.3.0.538) and IBM SPSS Statistics (version number 19.0) were used for all statistical analyses. Data were expressed as bar graphs (mean ± SD) of at least three independent experiments. Statistical analyses were performed using Student's *t* test or one-way ANOVA on the basis of the number of groups compared. A paired t test was used for paired samples.Multiple linear regression performed using SPSS software (SPSS).The multiple linear graphs were constructed using MATLAB visualisation function (slice). The polynomial functions were constructed using MATLAB fit function(polyfit). Error bars:bars donate S.D. *$p < 0.05$,**$p < 0.01$, ^$p < 0.05$, ^^$p < 0.01$, $^{\#}p < 0.05$, $^{\#\#}p < 0.01$, without significant difference (ns).